Journal of Computational Physics **170,** 498–522 (2001)
doi:10.1006/jcph.2001.6746, available online at http://www.idealibrary.com on IDEAL®

Completely Conservative and Oscillationless Semi-Lagrangian Schemes for Advection Transportation

Feng Xiao*,‡ and Takashi Yabe†

*Department of Energy Sciences, Tokyo Institute of Technology, 4259 Nagatsuta, Midori-ku, Yokohama, 226-8502 Japan; †Department of Mechanical Engineering and Science, Tokyo Institute of Technology, 2-12-1 O-okayama, Meguro-ku, Tokyo, 152-8552 Japan; and ‡Frontier Research System for Global Change, SEAVANS North, 1-2-1 Shibaura Minato-ku, Tokyo, 105-6791 Japan
E-mail: xiao@es.titech.ac.jp, yabe@mech.titech.ac.jp

Received February 21, 2000; revised September 5, 2000

In this paper, we present a new type of semi-Lagrangian scheme for advection transportation equation. The interpolation function is based on a cubic polynomial and is constructed under the constraints of conservation of cell-integrated average and the slope modification. The cell-integrated average is defined via the spatial integration of the interpolation function over a single grid cell and is advanced using a flux form. Nonoscillatory interpolation is constructed by choosing proper approximation to the cell-center values of the first derivative of the interpolation function, which appears to be a free parameter in the present formulation. The resulting scheme is exactly conservative regarding the cell average of the advected quantity and does not produce any spurious oscillation. Oscillationless solutions to linear transportation problems were obtained. Incorporated with an entropy-enforcing numerical flux, the presented schemes can accurately compute shocks and sonic rarefaction waves when applied to nonlinear problems.

Key Words: atmospheric modeling; computational algorithm; semi-Lagrangian scheme; linear and nonlinear transportation equations; mass conservation; shock wave.

1. INTRODUCTION

Semi-Lagrangian schemes, as indicated by the terminology, describe fluid evolution based on a reference frame moving with an individual parcel of fluid like a fully Lagrangian method but make use of an Eulerian computational grid and choose the set of the parcels at every time step so that all the fluid parcels arrive at each grid point of the regularly spaced Eulerian mesh at the next time step. As an efficient and accurate approach to computing the advection process, semi-Lagrangian schemes have been extensively studied and widely

0021-9991/01 $35.00

incorporated into numerical models for atmospheric flows during the past decades. Surveys of such a topic were given by Staniforth and Côté [25] and Smolarkiewicz and Pudykiewicz [24].

A semi-Lagrangian scheme in a one-dimensional flow field involves the numerical manipulations to solve the following differential equations for any physical variable $f(x, t)$,

$$\frac{df}{dt} = G(x, t) \tag{1}$$

and

$$\frac{dx}{dt} = u(x, t), \tag{2}$$

where t refers to the time, x is the spatial coordinate, u is the flow speed, and G refers to the source terms. Here, the total derivative is defined as

$$\frac{\partial}{\partial t} + u\frac{\partial}{\partial x}. \tag{3}$$

A semi-Lagrangian method usually makes use of the solution as a Lagrangian invariant at any instant t,

$$f(x, t) = f(\hat{x}, t - \Delta t), \tag{4}$$

where $\hat{x}$ denotes the departure point of a trajectory that originates at $t - \Delta t$ and arrives at x after Δt. As mentioned above, the end point x is chosen to coincide with a grid point, but the departure point $\hat{x}$ is not in general a grid point. Thus, the following three tasks always need to be done for any semi-Lagrangian scheme: (1) approximate the trajectory for all the parcels which arrive at grid points, (2) construct the interpolation function for $f(x, t - \Delta t)$ over the cell that covers the departure point of the trajectory, and (3) estimate the source terms G along the trajectory during the time integration from $t - \Delta t$ to t.

As discussed in [5], the back trajectory can be calculated with a second-order accuracy using a Runge–Kutta type scheme. The estimation of the source or forcing terms G, however, is a topic that is closely related to the physical problem to be solved, and some well-established methods, such as the trapezoidal method and the second-order Adams–Bashforth method, exist for practical applications. The construction of the interpolation for physical variable $f(x, t)$ remains the most active field for investigation since the first appearance of the semi-Lagrangian schemes and still attracts the interest of researchers. So far emphasis has been given to the numerical properties, such as accuracy [9, 15, 22, 33, 34], monotonicity [2, 30, 31, 32], and locality [31, 33, 34].

Unlike most Eulerian methods, which are derived by using control volume or cell-integrated average, the Lagrangian invariant solution used in a semi-Lagrangian scheme is based only on spatial points and is usually cast in a nonconservation form. Because of the intrinsic difficulties in introducing a conservation formulation in a semi-Lagrangian scheme, few studies on the conservation of the semi-Lagrangian schemes have been reported so far in the literature. A quasiconservative semi-Lagrangian advection scheme is proposed in [21] where a semi-Lagrangian scheme is derived by weighting the flux-corrected transport (FCT) method [3, 37] and a higher order interpolation. The weight is iteratively determined so that the conservation of the total amount of the advected quantity is enforced. As the

conservation and the positivity of the advected physical field are important or appear essential in many applications, development of a semi-Lagrangian scheme that guarantees these properties should be worth further efforts.

A semi-Lagrangian method that conserves exactly the transported physical field has been recently developed in [27, 35] by using the CIP (*constrained interpolation profile*) concept. The word "CIP" is originally the abbreviation of *cubic interpolated propagation*, a numerical scheme proposed by one of the authors for the linear scalar advection equation [33, 34]. Since *constrained interpolation profile* provides a more general concept that allows a larger variety or a wider spectrum of the numerical techniques to be involved in constructing a semi-Lagrangian scheme, we adopt CIP as a phrase standing for *constrained interpolation profile*. The original CIP method falls naturally into this extended concept of CIP as a subset. The original CIP method (see [33, 34]) is constructed on the basis of a cubic polynomial function. The first-order spatial derivatives of the interpolation function are assumed to follow a set of governing equations derived by differentiating the advection equation with respect to the spatial coordinates. These derivatives, according to the current interpretation of CIP, give constraints on the interpolation function. This scheme is completely different from conventional semi-Lagrangian methods regarding the computation of derivatives. In the latter methods, the gradient is calculated based on the function values at neighboring grid points either by assuming the continuity of the quantity, the first and sometimes the second-order derivatives of the quantity at the mesh boundaries [22], or by using approximations based on local grid points [30]. By a special treatment of the first derivatives of the interpolation function, the CIP method achieves a compact form that uses only one mesh cell to construct the interpolation profile.

Interpreting CIP as *constrained interpolation profile* implies that any physically or numerically meaningful treatment can be applied in developing a scheme. Accordingly, the interpolations for $f(x, t)$ can be constructed under some desired constraints to make the resulting scheme possess certain qualities. In [27] and [35], a constraint of the conservation relation for cell-integrated average is imposed at the stage to determine the piecewise interpolation functions. The resulting schemes, namely, CIP–CSL4 (constrained interpolation profile–conservative semi-Lagrangian scheme with fourth-order polynomial function) and CIP–CSL2 (constrained interpolation profile–conservative semi-Lagrangian scheme with second-order polynomial function), conserve exactly the cell-integrated average of the transported field.

In this paper, we propose another class of schemes called CIP–CSL3 (constrained interpolation profile–conservative semi-Lagrangian scheme with third-order polynomial function) using the CIP concept. The CIP–CSL3 schemes are constructed from a cubic polynomial. In addition to the conservation constraint used in the CIP–CSL2 and CIP–CSL4, the slope (first-order derivative) of the interpolation function at the middle point of a mesh cell is also introduced as another constraint on the interpolation function. The slope at the cell center can be easily approximated from a reconstruction procedure, and this allows manipulations, i.e., slope limiters, to make the interpolation oscillationless.

In Section 2, the fundamental CIP–CSL3 formulation is described, and some practical schemes are obtained by choosing different formulas for computing the slope. Numerical results for both the linear scalar advection equation and the Burgers equation are given in Section 3. Implementation with large CFL number is described in Section 4, and the paper ends with some concluding remarks in Section 5.

2. THE CIP–CSL3 SCHEMES

The model equation to be considered is a transportation equation in one dimension,

$$\frac{\partial f}{\partial t} + \frac{\partial}{\partial x}(uf) = 0, \tag{5}$$

where t refers to the time, x is the spatial coordinate, u is the characteristic speed, and f is the transported quantity.

The above equation in fact states a conservation law of $f(x, t)$ and can be recast into an integral form over any space–time control volume $[x, x + \Delta x] \times [t, t + \Delta t]$ as

$$\int_x^{x+\Delta x} f(x_1, t + \Delta t)\, dx_1 - \int_x^{x+\Delta x} f(x_1, t)\, dx_1 = -\left[\int_t^{t+\Delta t} f(x + \Delta x, t_1)u(x + \Delta x, t_1)\, dt_1 - \int_t^{t+\Delta t} f(x, t_1)u(x, t_1)\, dt_1\right]. \tag{6}$$

It is convenient to make use of the conservation form of (5) or (6) in constructing a finite-difference or finite-volume method via an Eulerian representation, and the resulting numerical formulation is in general automatically conservative. However, in applying a semi-Lagrangian calculation, Eq. (5) has to be written in a form as (1)

$$\frac{df}{dt} = -f\frac{\partial u}{\partial x}. \tag{7}$$

The only forcing term in this case is the divergence of the velocity field, and the semi-Lagrangian calculation is in general divided into a two-step procedure as

$$\tilde{f}(x, t) = f(x - u\Delta t, t - \Delta t) \tag{8}$$

and

$$f(x, t) = \tilde{f}(x, t) - \Delta t\, \tilde{f}(x, t)\frac{\partial u}{\partial x}. \tag{9}$$

It is obvious that this solution procedure does not necessarily guarantee the conservation of the advected quantity f as stated in (5) and (6). Nevertheless, an alternative way to enforce the conservation of a scheme in semi-Lagrangian form, can be devised by employing the conservation law as a constraining condition to the interpolation function.

We start from the given data $f(x_1), f(x_2), \ldots f(x_i) \ldots f(x_N)$ with $x_1 < x_2 < \cdots < x_i < \cdots < x_N$, which denote the numerical solution of Eq. (5), $\{f_i^n\}$, over the computational domain at n time steps ($t = t^n$), and make use of a piecewise cubic polynomial function, as in the original CIP method [33].

As with any other semi-Lagrangian schemes, the scheme we will discuss in this paper can bear a large time step only if one tracks back, according to the trajectory, to the corresponding departure point and constructs the interpolation profile over the mesh cell covering the departure point (see Section 4). For the sake of simplicity and without losing generality, the following discussions will be based on the neighboring cell of the grid point of interest.

The ith piece of the interpolation function is constructed over upwind stencils. Left-bias and right-bias components are then written as

$$F_i^L(x) = f(x_i) + c_{1i}^L(x - x_i) + c_{2i}^L(x - x_i)^2 + c_{3i}^L(x - x_i)^3, \quad \text{for} \quad x \in [x_{i-1}, x_i] \tag{10}$$

and

$$F_i^R(x) = f(x_i) + c_{1i}^R(x - x_i) + c_{2i}^R(x - x_i)^2 + c_{3i}^R(x - x_i)^3, \quad \text{for} \quad x \in [x_i, x_{i+1}]. \tag{11}$$

We consider a construction over the left-side stencils of grid i with $x_{i-1} \le x \le x_i$ and define the left-side interpolation function as that in (10). It implies the case of $u \ge 0$. From the continuity of $F_i^L(x)$ at the two ends of the cell, we have

$$F_i^L(x_i) = f^n(x_i) \tag{12}$$

and

$$F_i^L(x_{i-1}) = f^n(x_{i-1}). \tag{13}$$

As in the CIP–CSL2 method, a constraint for the conservation of cell-integrated average is imposed as

$$\int_{x_{i-1}}^{x_i} F_i^L(x)\,dx = \rho_{i-\frac{1}{2}}^n. \tag{14}$$

Another constrained condition for the interpolation construction is imposed on the first-order derivative of $F_i^L(x)$, $dF_i^L(x)/dx$, at the middle point of the cell,

$$\frac{dF_i^L(x)}{dx} = d_{i-\frac{1}{2}}^n. \tag{15}$$

In terms of f_i^n, f_{i-1}^n, $d_{i-1/2}^n$, and $\rho_{i-1/2}^n$, the polynomial (10) can be completely determined from (12)–(14), and the coefficients read

$$\begin{cases} c_{1i}^L = -\frac{6}{\Delta x_{i-\frac{1}{2}}^2}\rho_{i-\frac{1}{2}}^n - \frac{6}{\Delta x_{i-\frac{1}{2}}} f_i^n - 2d_{i-\frac{1}{2}}^n, \\ c_{2i}^L = -\frac{6}{\Delta x_{i-\frac{1}{2}}^3}\rho_{i-\frac{1}{2}}^n + \frac{3}{\Delta x_{i-\frac{1}{2}}^2}\left(3f_i^n - f_{i-1}^n\right) - \frac{6}{\Delta x_{i-\frac{1}{2}}} d_{i-\frac{1}{2}}^n, \\ c_{3i}^L = \frac{4}{\Delta x_{i-\frac{1}{2}}^3}\left(f_i^n - f_{i-1}^n\right) - \frac{4}{\Delta x_{i-\frac{1}{2}}^2} d_{i-\frac{1}{2}}^n, \end{cases} \tag{16}$$

where $\Delta x_{i-1/2} = x_i - x_{i-1}$.

Analogously, the coefficients for the right-bias interpolation function $F_i^R(x)$ read

$$\begin{cases} c_{1i}^R = \frac{6}{\Delta x_{i+\frac{1}{2}}^2}\rho_{i+\frac{1}{2}}^n - \frac{6}{\Delta x_{i-\frac{1}{2}}} f_i^n - 2d_{i+\frac{1}{2}}^n, \\ c_{2i}^R = -\frac{6}{\Delta x_{i+\frac{1}{2}}^3}\rho_{i+\frac{1}{2}}^n + \frac{3}{\Delta x_{i+\frac{1}{2}}^2}\left(3f_i^n - f_{i+1}^n\right) + \frac{6}{\Delta x_{i+\frac{1}{2}}} d_{i+\frac{1}{2}}^n, \\ c_{3i}^R = -\frac{4}{\Delta x_{i+\frac{1}{2}}^3}\left(f_i^n - f_{i+1}^n\right) - \frac{4}{\Delta x_{i+\frac{1}{2}}^2} d_{i+\frac{1}{2}}^n. \end{cases} \tag{17}$$

Once the interpolation function is determined, the numerical solution of f at time step $n + 1$ is updated as

$$\tilde{f}_i = \begin{cases} F_i^L(x_i - u\Delta t), & \text{if } u > 0, \\ F_i^R(x_i - u\Delta t), & \text{if } u < 0, \end{cases} \tag{18}$$

and

$$f_i^{n+1} = \tilde{f}_i - \frac{\Delta t}{\Delta x_{i-\frac{1}{2}} + \Delta x_{i+\frac{1}{2}}} \tilde{f}_i (u_{i+1} - u_{i-1}). \tag{19}$$

Following [27, 35], the cell-integrated average ρ is advanced by the conservative relation

$$\rho_{i-\frac{1}{2}}^{n+1} = \rho_{i-\frac{1}{2}}^{n} - (g_i - g_{i-1}), \tag{20}$$

where g_i represents the flux of ρ across boundary $x = x_i$ during $t^{n+1} - t^n$ and is computed as

$$g_i = \int_{t^n}^{t^{n+1}} \left[\min(0, u) F_i^R (x_i - u(t - t^n)) + \max(0, u) F_i^L (x_i - u(t - t^n)) \right] dt. \tag{21}$$

Assuming that velocity u remains constant during time interval $t^{n+1} - t^n = \Delta t$ yields

$$\begin{aligned} g_i = &-\min(0, \xi) \left(f_i^n + \frac{1}{2} c_{1i}^R \xi + \frac{1}{3} c_{2i}^R \xi^2 + \frac{1}{4} c_{3i}^R \xi^3 \right) \\ &-\max(0, \xi) \left(f_i^n + \frac{1}{2} c_{1i}^L \xi + \frac{1}{3} c_{2i}^L \xi^2 + \frac{1}{4} c_{3i}^L \xi^3 \right), \end{aligned} \tag{22}$$

where $\xi = -u_i \Delta t$.

The slope of the interpolation function at the cell center $d_{i-1/2}^n$ remains a free parameter to be determined. It is this parameter that provides us a way to modify the interpolation function for suppressing numerical oscillation. To make the resulting scheme more local, we construct $d_{i-1/2}^n$ using the cell center values $f_{1/2}^n, f_{3/2}^n, \cdots f_{i-1/2}^n \cdots$.

The value of the interpolation function at the cell-central point $x = x_{i-1/2}$ can be found immediately from (10) as

$$f_{i-\frac{1}{2}}^n = \frac{3}{2\Delta x_{i-\frac{1}{2}}} \rho_{i-\frac{1}{2}}^n - \frac{1}{4} \left(f_i^n + f_{i-1}^n \right). \tag{23}$$

There are many choices for evaluating $d_{i-1/2}^n$. The well-known approximations for first-order derivatives, such as those proposed in [1], [6], or [10], can be the candidates in some practical situations. In the present paper, we will define and discuss several CIP–CSL3 type schemes by choosing different approximations to $d_{i-1/2}^n$.

2.1. *The CIP–CSL3_HYMAN Scheme*

Using the approximation proposed by Hyman [10], we compute $d_{i-1/2}^n$ as

$$d_{i-\frac{1}{2}}^n = \frac{-f_{i+\frac{3}{2}}^n + 8 f_{i+\frac{1}{2}}^n - 8 f_{i-\frac{3}{2}}^n + f_{i-\frac{5}{2}}^n}{-\Delta x_{i+1} + 7\Delta x_i + 7\Delta x_{i-1} - \Delta x_{i-2}}, \tag{24}$$

where $\Delta x_i = \frac{1}{2}\Delta x_{i+1/2} + \frac{1}{2}\Delta x_{i-1/2}$.

The resulting scheme is called the CIP–CSL3_HYMAN scheme. The Hyman approximation has fourth-order accuracy for a smooth solution but will cause computationally spurious oscillation in the presence of a discontinuity or large gradient.

The Hyman approximation is not an oscillation-suppressing formulation. We include it in the present paper to illustrate that the choice of an approximation to $d_{i-1/2}^n$ essentially affects the interpolation profile and the numerical solution. As with the following two candidates for computing $d_{i-1/2}^n$, an oscillationless solution can be obtained by choosing proper slope limiters for $d_{i-1/2}^n$.

2.2. *The CIP–CSL3_UNO Scheme*

We call a scheme CIP–CSL3_UNO if a UNO reconstruction is used to evaluate the derivative $d^n_{i-1/2}$.

From [8], a UNO construction for $d^n_{i-1/2}$ can be written as

$$d^n_{i-\frac{1}{2}} = \text{minmod}\left(S^+_{i-\frac{1}{2}}, S^-_{i-\frac{1}{2}}\right), \tag{25}$$

where the minimum modulus function is defined as

$$\text{minmod}(a,b) = \begin{cases} \text{m}(a,b), & \text{if } a \text{ and } b \text{ have same sign,} \\ 0, & \text{if } a \text{ and } b \text{ have opposite signs,} \end{cases} \tag{26}$$

and

$$\text{m}(a,b) = \begin{cases} a, & \text{if } |a| \le |b|, \\ b, & \text{otherwise.} \end{cases} \tag{27}$$

The piecewise-quadratic reconstruction functions are defined as

$$S^+_{i-\frac{1}{2}} = f\left[x_{i-\frac{1}{2}}, x_{i+\frac{1}{2}}\right] - \Delta x_i \text{minmod}\left(f\left[x_{i-\frac{3}{2}}, x_{i-\frac{1}{2}}, x_{i+\frac{1}{2}}\right], f\left[x_{i-\frac{1}{2}}, x_{i+\frac{1}{2}}, x_{i+\frac{3}{2}}\right]\right) \tag{28}$$

and

$$S^-_{i-\frac{1}{2}} = f\left[x_{i-\frac{3}{2}}, x_{i-\frac{1}{2}}\right] - \Delta x_{i-1} \text{minmod}\left(f\left[x_{i-\frac{5}{2}}, x_{i-\frac{3}{2}}, x_{i-\frac{1}{2}}\right], f\left[x_{i-\frac{3}{2}}, x_{i-\frac{1}{2}}, x_{i+\frac{1}{2}}\right]\right). \tag{29}$$

The first and second Newton-divided differences are defined as

$$f\left[x_{i-\frac{1}{2}}, x_{i+\frac{1}{2}}\right] = \frac{f^n_{i+\frac{1}{2}} - f^n_{i-\frac{1}{2}}}{\Delta x_i} \tag{30}$$

and

$$f\left[x_{i-\frac{1}{2}}, x_{i+\frac{1}{2}}, x_{i+\frac{3}{2}}\right] = \frac{1}{\Delta x_{i+1} + \Delta x_i}\left(\frac{f^n_{i+\frac{3}{2}} - f^n_{i+\frac{1}{2}}}{\Delta x_{i+1}} - \frac{f^n_{i+\frac{1}{2}} - f^n_{i-\frac{1}{2}}}{\Delta x_i}\right). \tag{31}$$

The UNO reconstruction procedure selects a line over $[x_{i-1}, x_i]$ that is bounded by

$$f_{i-\frac{1}{2}} + f\left[x_{i-\frac{1}{2}}, x_{i+\frac{1}{2}}\right]\left(x - x_{i-\frac{1}{2}}\right) \tag{32}$$

and

$$f_{i-\frac{1}{2}} + f\left[x_{i-\frac{3}{2}}, x_{i-\frac{1}{2}}\right]\left(x - x_{i-\frac{1}{2}}\right). \tag{33}$$

The UNO reconstruction [8] has a uniform second-order accuracy and appears less oscillatory in the presence of discontinuity.

Instead of the averaging in the UNO reconstruction, essentially nonoscillatory (ENO) reconstruction [7] can also be applied by carefully choosing a single piecewise-quadratic

interpolation which should be the one closest to the line which lies between (32) and (33). Furthermore, more generalized reconstructions using averaging techniques, such as weighted ENO (WENO), can be devised by combining the candidate polynomial interpolations (see Liu, *et al.* [14] and Jiang and Shu [11]).

2.3. *The CIP–CSL3_CW Scheme*

In this scheme we adopt the approximation suggested by Collela and Woodward [4] as

$$d^n_{i-\frac{1}{2}} = \begin{cases} \min\left(\left|\delta f^n_{i-\frac{1}{2}}\right|, 2\left|f^n_{i+\frac{1}{2}} - f^n_{i-\frac{1}{2}}\right|, 2\left|f^n_{i-\frac{1}{2}} - f^n_{i-\frac{3}{2}}\right|\right)\mathrm{sgn}\left(\delta f^n_{i-\frac{1}{2}}\right)\Big/\Delta x_{i-\frac{1}{2}}, \\ \text{if } \left(f^n_{i+\frac{1}{2}} - f^n_{i-\frac{1}{2}}\right)\left(f^n_{i-\frac{1}{2}} - f^n_{i-\frac{3}{2}}\right) > 0; \\ 0, \quad \text{otherwise.} \end{cases} \tag{34}$$

The average slope $\delta f^n_{i-\frac{1}{2}}$ is given by

$$\delta f^n_{i-\frac{1}{2}} = \frac{\Delta x_{i-\frac{1}{2}}}{\Delta x_{i-\frac{3}{2}} + \Delta x_{i-\frac{1}{2}} + \Delta x_{i+\frac{1}{2}}}\left(\frac{2\Delta x_{i-\frac{3}{2}} + \Delta x_{i-\frac{1}{2}}}{\Delta x_{i-\frac{1}{2}} + \Delta x_{i+\frac{1}{2}}}\left(f^n_{i+\frac{1}{2}} - f^n_{i-\frac{1}{2}}\right)\right.$$
$$\left. + \frac{\Delta x_{i-\frac{1}{2}} + 2\Delta x_{i+\frac{1}{2}}}{\Delta x_{i-\frac{3}{2}} + \Delta x_{i-\frac{1}{2}}}\left(f^n_{i-\frac{1}{2}} - f^n_{i-\frac{3}{2}}\right)\right). \tag{35}$$

This reconstruction, referred to as CW reconstruction hereafter, is a third-order-accurate approximation in smooth regions. As we will show later, the modified slope computed from (34) is able to effectively avoid oscillations in the presence of jump discontinuities, but it tends to flatten a peak and create a plateau in the area where $\delta f^n_{i-1/2}$ changes sign.

2.4. *Outline of the Computational Procedure*

As discussed in the previous sections, a CIP–CSL3 type scheme can be coded via the following steps:

- Construct the interpolation function:

  (i) compute $d^n_{i-1/2}$ from $\{f^n_{i-1/2}\}$ using a slope approximation, i.e., any of (24), (25), (34), or others and

  (ii) determine the cubic polynomial (10) or (11) in terms of f^n_i, f^n_{i-1}, $d^n_{i-1/2}$, and $\rho^n_{i-1/2}$ by (16) or (17).
- Advance the solution:

  (i) calculate the semi-Lagrangian solution of f by (18),

  (ii) correct f according to velocity divergence via (19), and

  (iii) predict the cell-integrated average ρ using the exactly conservative formulation (20).

Before closing this section, we want to remark on a few apparent differences between our methods and other schemes which also use interpolation constructions, such as the MUSCL scheme [28, 29] and the piecewise parabolic method (PPM) [4]. In these other schemes, a linear (MUSCL) or a parabolic (PPM) function is used to construct the interpolation function which is then used to evaluate the numerical flux with second- or third-order accuracy. All the construction procedures start from the cell-average values. The values of the dependent

variable at cell interfaces are computed from the neighboring cell averages and modified to enforce the monotonicity. In addition to a slope modification, the modification of the values at cell interfaces proves essential to get an oscillationless solution; otherwise the dispersion errors of the numerical solution will be significant. The constructed piecewise interpolation functions are in general not connected across cell interfaces. In our schemes, the values at the cell interfaces (the grid points in our terminology) are computed based on a semi-Lagrangian approach and no modification is involved. Using the semi-Lagrangian solution makes the dispersion errors less and more local. This can be easily understood if one consults the numerical results of the CSL2 scheme (see Section 3) where no modification was done to either slope or cell-interface values. In the CSL3_UNO and the CSL3_CW, only the slope at the cell center was modified. Thus the pieces of the interpolation functions are connected and make a profile with a smoothness of at least C^0.

3. NUMERICAL TESTS

The numerical schemes proposed in Section 2 were tested on both linear and nonlinear scalar transportation problems. Test problems were chosen to illustrate the numerical properties of the presented schemes, such as phase and amplitude errors, mass conservation, oscillatory errors across discontinuities, smearing and dispersion of contact discontinuities, capacities of capturing shocks, and expansion fans. We included the CIP–CSL2 [35] scheme as well for comparison.

In all the calculations presented in this paper, an evenly spaced mesh with $\Delta x = 0.01$ and a fixed increment for time integration $\Delta t = 0.002$ are used.

3.1. *Linear Scalar Transportation*

We consider one-dimensional linear initial problems as

$$\frac{\partial f}{\partial t} + \frac{\partial}{\partial x}(uf) = 0, \qquad (t, x) \in [0, \infty) \times (-\infty, +\infty) \tag{36}$$

with different initial conditions

$$f(x, 0) = f^0(x), \qquad x \in (-\infty, +\infty).$$

3.1.1. Test 1. To examine phase and amplitude errors, a sine function

$$f^0(x) = \sin(5\pi x) \tag{37}$$

was used as the initial profile. A constant velocity $u = 1.0$ was set throughout the computational domain.

As displayed in Fig. 1, all tested schemes recovered the exact solution perfectly except the CIP–CSL3_CW which flattens the ridge of the wave due to the slope limiter. The PPM [4] which uses the same slope limiter produces a similar solution with flattened peaks. The results from the other three schemes are visually identical. Since all schemes have higher than second-order accuracy, the amplitude of the smooth solution is well preserved. As a type of semi-Lagrangian method, the phase errors are completely eliminated by using the Lagrangian invariant solution of the linear advection equation.

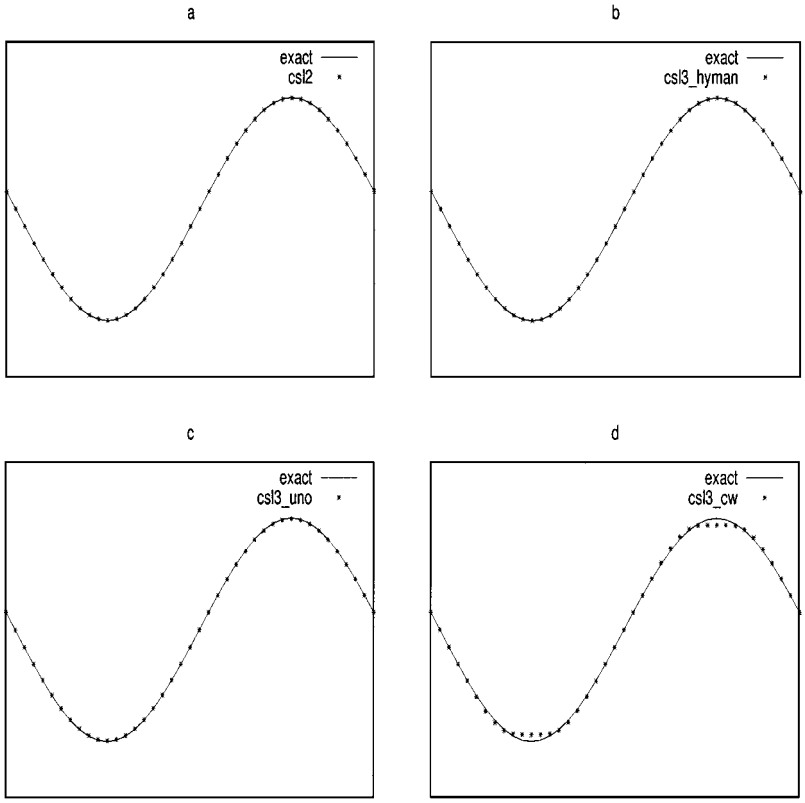

FIG. 1. A transported sine wave after 1000 step calculations with the CIP–CSL2 scheme (a), the CIP-CSL3_HYMAN scheme (b), the CIP–CSL3_UNO scheme (c), and the CIP–CSL3_CW scheme (d).

Resolution refinement tests were carried out using a sine function with wavelengths of $10\Delta x$, $20\Delta x$, and $40\Delta x$.

Following Takacs [26] and Bermejo and Staniforth [2], a measure of the total error based on a l_2 norm is given as

$$E_{l_2} = \frac{1}{N}\sum_{i=1}^{N}\left(f_i^n - f_i^{exact}\right)^2, \tag{38}$$

where N is the total number of grid points.

The numerical errors are given in Table I. We included the results of the PPM as well for comparison. The CIP–CSL3_HYMAN produces the best solutions for all wavelengths. The PPM shows an accuracy between CIP–CSL3_UNO and CIP–CSL3_CW. The convergence rates of the schemes were also evaluated and shown in Table II. The rates for all the tested schemes show a decline in the long-wave regime, where the sine wave is well represented by the schemes. Especially, CIP–CSL2 and CIP–CSL3_HYMAN show a significantly saturated convergence for the smooth solution of long waves. CIP–CSL3_UNO has the best convergence rate for all the wavelengths. The PPM clips the sharp peaks and gives the lowest convergence rate in the short-wave regime.

TABLE I
Grid Refinement Tests of Different Schemes

Wavelength	$10\Delta x$	$20\Delta x$	$40\Delta x$
CSL2	1.26×10^{-2}	1.44×10^{-4}	3.46×10^{-6}
CSL3_HYMAN	2.73×10^{-3}	3.95×10^{-5}	2.15×10^{-6}
CSL3_UNO	1.02×10^{-1}	9.32×10^{-4}	9.42×10^{-6}
CSL3_CW	2.97×10^{-1}	7.51×10^{-3}	2.84×10^{-4}
PPM	1.87×10^{-1}	5.37×10^{-3}	1.76×10^{-4}

Note. A sine wave with different wavelengths was computed. Displayed are the errors defined by $E_{l_2} = \frac{1}{N}\sum_{i=1}^{N}(f_i^n - f_i^{exact})^2$.

3.1.2. Test 2. This problem is the transportation of a square wave. The conditions are the same as in the previous example except that the initial profile is defined as

$$f^0(x) = \begin{cases} 1, & |x| \le 0.15, \\ 0, & \text{otherwise.} \end{cases} \tag{39}$$

The computed results of the CIP–CSL2, CIP–CSL3_HYMAN, CIP–CSL3_UNO, and CIP–CSL3_CW at $t = 2$ are plotted in Fig. 2. As expected, without a smoothing constraint, the CSL2 and the CIP–CSL3_HYMAN methods produced significant spurious undershoots and overshoots near the large gradients. The profile from the CIP–CSL3_HYMAN method looks somewhat similar to that of the CSL2, but it has steeper jumps at the discontinuities because of the use of a higher order interpolation function. Constrained by the oscillation-suppressing reconstructions, i.e., the UNO and the CW reconstructions, CIP–CSL3_UNO and CIP–CSL3_CW give well-regulated results. The profiles are effectively bounded. Compared with the CIP–CSL3_UNO, the CIP–CSL3_CW seems to be able to reinforce the initial sharpness.

Further examinations on the conservation qualities, numerical oscillations, and overall computational errors of the presented schemes can be carried out with the aid of Table III. To compare the performances of the schemes in mass conservation and the numerical oscillation, we calculated the rates of the first and the second moments of the numerical solution at instant t against the initial values defined as $\mathrm{RFM} = \int f(t) / \int f(0)$ and $\mathrm{RSM} = \int f^2(t) / \int f^2(0)$. The maximum and the minimum of the computed values are inspected as well.

TABLE II
Convergence Rates of Different Schemes

Wavelength	$[E_{l_2}(10\Delta x)/E_{l_2}(20\Delta x)]^{1/2}$	$[E_{l_2}(20\Delta x)/E_{l_2}(40\Delta x)]^{1/2}$
CSL2	9.35	6.45
CSL3_HYMAN	8.31	4.29
CSL3_UNO	10.46	9.95
CSL3_CW	6.29	5.14
PPM	5.9	5.52

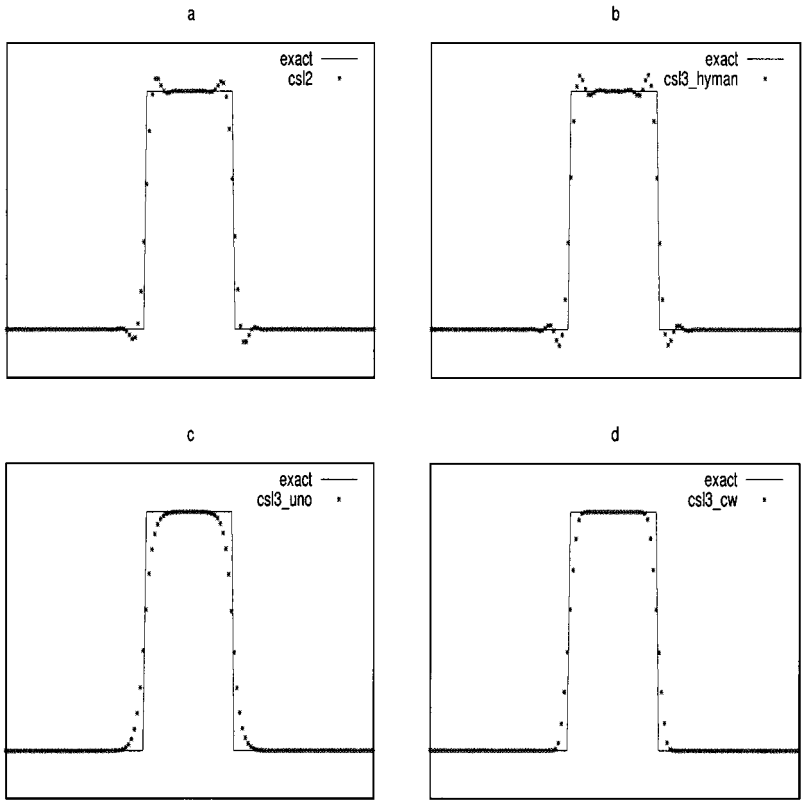

FIG. 2. Same as Fig. 1, but a square wave.

All the tested schemes conserve exactly the first moment. The second moment appears to have a larger loss with a more diffusive solution. Consistent with what is observed in Fig. 2, the CIP–CSL3_UNO and CIP–CSL3_CW completely avoid the numerical undershoot and overshoot, while the CIP–CSL2 and CIP–CSL3_HYMAN do not. The slope limiters used in UNO or in Collela and Woodward's reconstructions effectively suppress the spurious oscillation. With the most significant oscillatory errors, the CIP–CSL3_HYMAN shows the least diffused solution and appears superior in terms of the total errors. In this particular case,

TABLE III
Numerical Properties of Different Schemes on the Square Wave Transportation Problem

Scheme	RFM	RSM	MAX	min	E_{l_2}
CSL2	1.0	0.979	1.053	−0.053	1.758×10^{-3}
CSL3_HYMAN	1.0	0.986	1.068	−0.068	1.558×10^{-3}
CSL3_UNO	1.0	0.916	1.0	0.0	2.791×10^{-3}
CSL3_CW	1.0	0.941	1.0	0.0	2.435×10^{-3}

Note. MAX and min indicate the highest and the lowest values produced by the schemes. Other quantities are defined as $E_{l_2} = \frac{1}{N}\sum_{i=1}^{N}(f_i^n - f_i^{exact})^2$, RFM $= \int f(t)/\int f(0)$, and RSM $= \int f^2(t)/\int f^2(0)$.

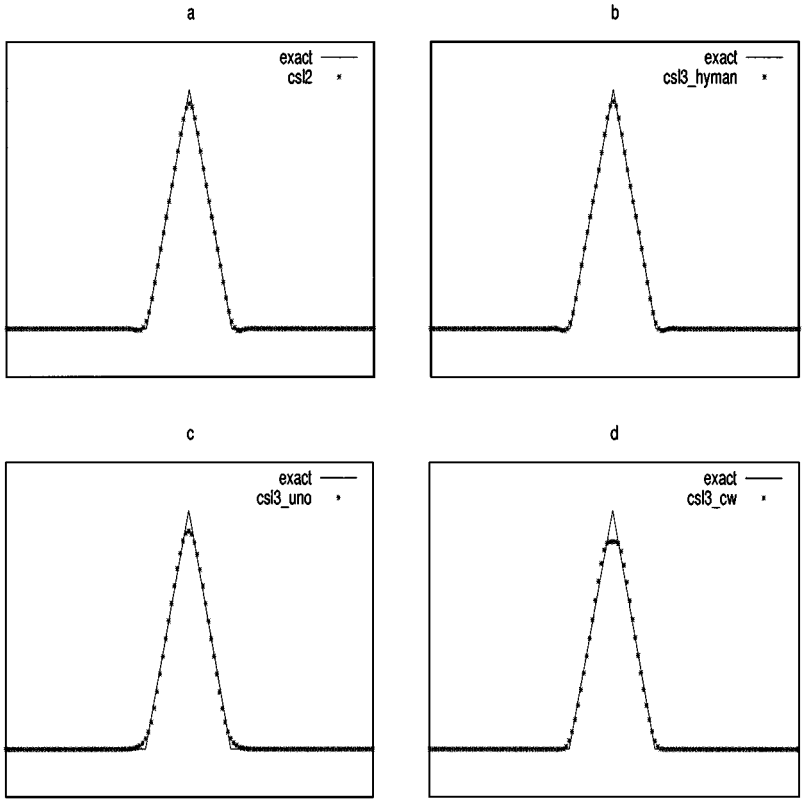

FIG. 3. Same as Fig. 1, but a triangular wave.

the CIP–CSL3_CW gives a good compromise between smearing the contact discontinuity and eliminating numerical oscillation.

3.1.3. Test 3. The transportation of a triangle wave, initially given as

$$f^0(x) = \begin{cases} 1 - \frac{|x|}{0.15}, & |x| \le 0.15, \\ 0, & \text{otherwise} \end{cases} \tag{40}$$

is computed in this case. The results at $t = 2$ are given in Fig. 3 and Table IV. Again, all schemes conserve the total transported mass. As can be expected, the CIP–CSL2 and the CIP–CSL3_HYMAN produce numerical undershoots but better preserve the sharp peak, while the CIP–CSL_UNO and the CIP–CSL3_CW result in a somewhat more smeared peak.

TABLE IV
Same as Table I, but for the Triangle Wave Transportation Problem

Scheme	RFM	RSM	MAX	min	E_{l_2}
CSL2	1.0	0.997	0.940	−0.008	1.770×10^{-5}
CSL3_HYMAN	1.0	0.999	0.950	−0.007	1.278×10^{-5}
CSL3_UNO	1.0	0.984	0.912	0.0	5.792×10^{-5}
CSL3_CW	1.0	0.987	0.869	0.0	9.844×10^{-5}

TABLE V
Transportation of a Square Wave with a Variable Velocity Field

Scheme	RFM	RSM	MAX	min	E_{l_2}
CSL2	1.0	0.572	0.825	−0.054	1.672×10^{-3}
CSL3_HYMAN	1.0	0.578	0.857	−0.065	1.614×10^{-3}
CSL3_UNO	1.0	0.532	0.759	0.0	2.568×10^{-3}
CSL3_CW	1.0	0.544	0.781	0.0	2.413×10^{-3}

It is also observed that the CIP–CSL3_CW scheme causes the worst clip to the triangular peak, because the CW reconstruction tends to enforce the jump transition between two plateaus and a sharp corner is then always subjected to being flattened.

3.1.4. Test 4. A variable velocity field

$$u(x) = \frac{1}{1 + 0.5\sin(8\pi x)}$$

was used to test the conservations of the numerical schemes with a non-divergence-free velocity. A square wave

$$f^0(x) = \begin{cases} 1, & 0.1 \le x \le 0.13, \\ 0, & \text{otherwise} \end{cases}$$

is transported through the computational domain until $t = 1.7$. As shown in [23], an analytical solution to this problem can be found by solving $\frac{df}{f} = \frac{du}{u}$ along the characteristic curves. From Table V, we found that the total mass was exactly conserved even with the drastically changed velocity field. The CIP–CSL3_UNO and CIP–CSL3_CW give positive solutions. Also in Fig. 4, the solutions from CIP–CSL3_UNO and CIP–CSL3_CW appear much less oscillatory, although new extrema are physically permitted in this case because of the variable velocity. CIP–CSL3_HYMAN has the smallest l_2 errors but gives the most oscillatory solution.

3.2. *Burgers' Equation*

As discussed by Bermejo and Staniforth [2], because a conventional semi-Lagrangian scheme is a kind of method of characteristics, it fails in recognizing uniquely the characteristic curves which pass through a shock. A shock-fitting technique was then suggested to isolate the shock from the smooth region where a unique characteristic curve is attainable. However, a shock-fitting method proves to be difficult to apply to more complicated or multidimensional physical problems [19, 21].

It is currently well accepted that, instead of fitting a shock, capturing a shock using a conservative scheme is a more practical approach, since a local conservation, which is automatically satisfied if a piecewise flux form is used, guarantees the right shock placement [12].

We will show with the inviscid Burgers equation that the presented schemes, in spite of being of semi-Lagrangian type, are capable of correctly capturing shocks with the conservative constraint.

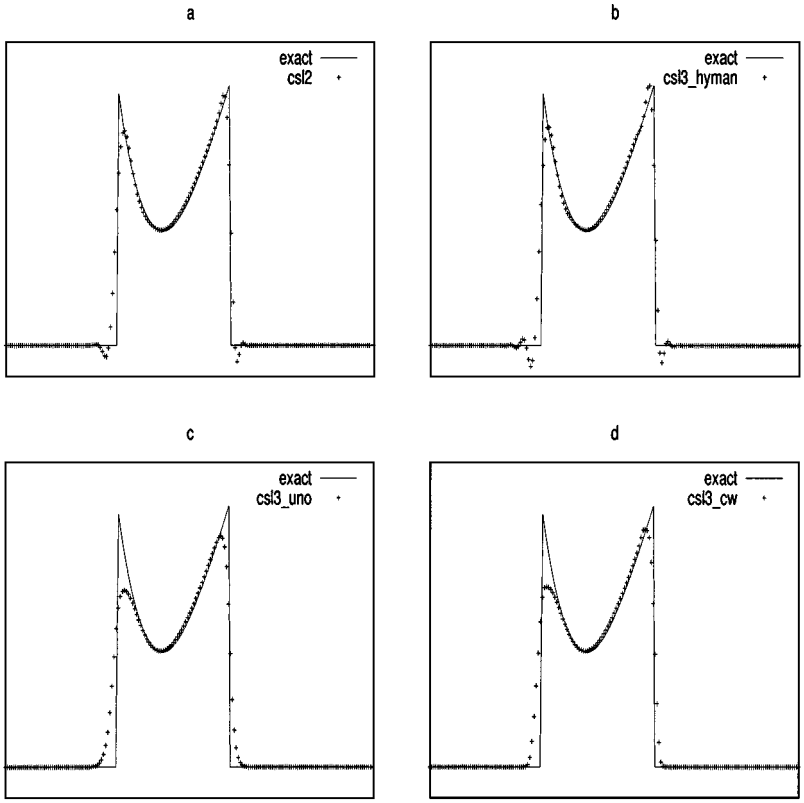

FIG. 4. Transportation of an initial square wave with a variable velocity field. Displayed are the results after 2000 step calculations with the CIP–CSL2 scheme (a), the CIP–CSL3_HYMAN scheme (b), the CIP–CSL3_UNO scheme (c), and the CIP–CSL3_CW scheme (d).

As a nonlinear transportation problem, the Burgers equation allows solutions such as the shock and the expansion fan. Being developed for a scalar conservation law, the presented schemes can be straightforwardly applied to the Burgers equation. We consider the inviscid Burgers equation

$$\frac{\partial u}{\partial t} + \frac{\partial H(u)}{\partial x} = 0, \tag{41}$$

where $H(u) = \frac{1}{2}u^2$ is the flux function.

To implement a semi-Lagrangian calculation, its advection form can be written as

$$\frac{\partial u}{\partial t} + a(u)\frac{\partial u}{\partial x} = 0. \tag{42}$$

There are many ways to determine the characteristic speed $a(u)$. Since semi-Lagrangian methods are based on a quasilinear solution procedure, accurately estimating the advection speed and the trajectory is not easy in a nonlinear case. In the present study, the advection velocity is defined as $a(u) = \partial H(u)/\partial u$. We use the values of u at cell centers to approximate $\partial H(u)/\partial u$. From (23), interpolation function readily provides the middle-point values.

Using a central difference, we have

$$(\partial H(u)/\partial u)_i = \frac{H\left(u_{i+\frac{1}{2}}\right) - H\left(u_{i-\frac{1}{2}}\right)}{u_{i+\frac{1}{2}} - u_{i-\frac{1}{2}}}. \tag{43}$$

Instead of using a two-step procedure, such as (8) and (9), the divergence correction is absorbed into the advection phase and u is solved by

$$u^{n+1}(x,t) = u^n(x - a(u^n)\Delta t, t - \Delta t). \tag{44}$$

After u^{n+1} is obtained, a flux modification similar to that suggested in [20] is adopted as

$$g_i = \begin{cases} \frac{1}{2}\min_{u^{n+1}\le u\le u^n} g(u)_i, & \text{if } u_{i+\frac{1}{2}} > u_{i-\frac{1}{2}} \\ \frac{1}{2}\max_{u^{n+1}\ge u\ge u^n} g(u)_i, & \text{if } u_{i+\frac{1}{2}} < u_{i-\frac{1}{2}}, \end{cases} \tag{45}$$

where

$$\begin{aligned} g(u)_i = &-\min[0,(ut)]\left[f_i^n + \frac{1}{2}c_{1i}^R(ut) + \frac{1}{3}c_{2i}^R(ut)^2 + \frac{1}{4}c_{3i}^R(ut)^3\right] \\ &-\max[0,(ut)]\left[f_i^n + \frac{1}{2}c_{1i}^L(ut) + \frac{1}{3}c_{2i}^L(ut)^2 + \frac{1}{4}c_{3i}^L(ut)^3\right]. \end{aligned} \tag{46}$$

Using (45), the cell-integrated average ρ^{n+1} is predicted from (20).

Remark. In a conventional high-resolution scheme, subgrid resolution is obtained through a reconstruction using cell-averaged values. The physical variable and the numerical flux are allowed to be discontinuous across a cell boundary, usually denoted by u_L and u_R. Hence any such constructed scheme appears to be able to readily use the numerical flux to get an entropy-consistent solution as discussed in [20]. The methods presented in this paper, however, have continuous reconstruction profiles at cell boundaries. Thus, any numerically entropy-consistent flux that is based on a Riemann problem cannot be directly implemented in our cases. Alternatively, since the dependent variable u is computed separately from the cell-integrated average ρ, we are provided with a possibility to evaluate the numerical flux by using the values of the dependent variable u at two different instants. Recalling that u is advanced via a Lagrangian invariant solution according to the characteristics, it is easy to understand that (45) functions equivalently as the formula discussed in [20].

3.2.1. Test 5. We repeated the sample problem calculated in [2, 21]. The initial profile is

$$u^0(x) = \frac{1}{4} + \frac{1}{2}\sin(\pi x). \tag{47}$$

The results at $t = 1.5$ from all presented schemes are plotted in Fig. 5. $t = 1.5$ is an instant far beyond the time required for the initially smooth profile to develop into a discontinuous shock. We found that all the schemes reproduced the correct shock position. Solutions from all schemes look quite similar except that some minor oscillations are observed behind the shocks from the CSL3_HYMAN scheme. We may attribute this to the interpolation function used in the reconstruction. The other two with UNO and CW reconstructions give oscillationless solutions.

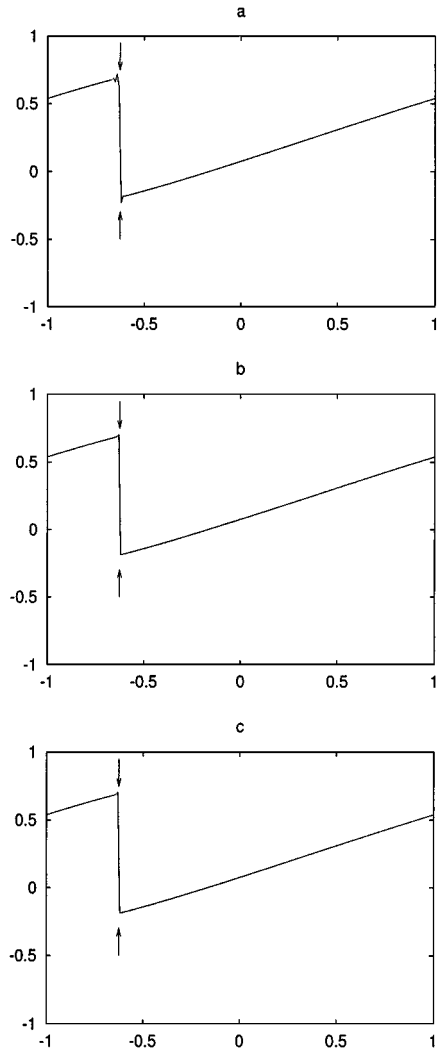

FIG. 5. Shock solution of Burger's equation at $t = 1.5$ from an initial sine wave (47). The arrows indicate the accurate shock position. Displayed are the results computed by the CIP–CSL3_HYMAN scheme (a), the CIP–CSL3_UNO scheme (b), and the CIP–CSL3_CW scheme (c).

3.2.2. Test 6. This example was used in [36] to test numerical schemes with shocks and sonic rarefaction wave. The initial profile is specified as a parabolic profile,

$$u^0(x-2.5) = \begin{cases} \max[0, (x-2.5)(1.5-x)], & x-2.5 \geq 0, \\ -u^0(x-2.5), & x-2.5 < 0. \end{cases} \tag{48}$$

The profile will create a left-moving shock and a right-moving shock, and an expansion region will develop between them. Figure 6 shows the outputs at $t = 2$ and $t = 12$. The numerical flux defined in (45) and (46) works extremely well with the shocks and the sonic rarefaction wave. Some ripples in the solution of CSL3_HYMAN immediately after the formation of the shock ($t = 2$) are observed, whereas CSL3_UNO and CSL3_CW give excellent results.

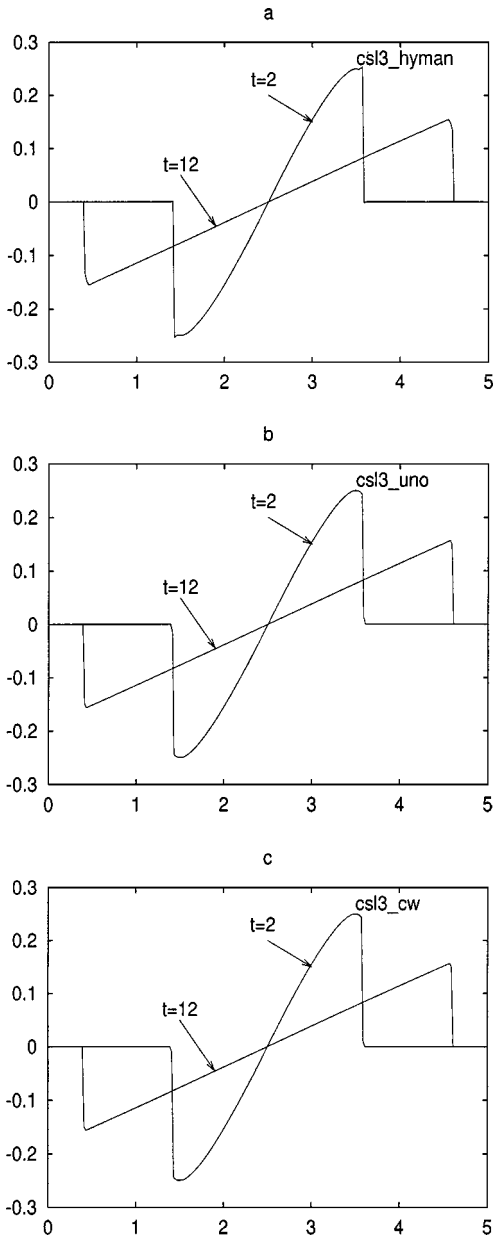

FIG. 6. Solution of the Burgers equation from an initial parabolic profile (48). Displayed are the results computed by the CIP–CSL3_HYMAN scheme (a), the CIP–CSL3_UNO scheme (b), and the CIP–CSL3_CW scheme (c).

3.2.3. Test 7. A more complicated initial condition (the same as that used in [36]) is specified as

$$u^0(x) = \begin{cases} 1.0, & 2.0 > x > 0.2, \\ -0.5, & 3.0 > x > 2.0, \\ -1.0, & 4.8 > x > 3.0, \\ 0.0, & \text{otherwise.} \end{cases} \tag{49}$$

A right-moving shock and a left-moving shock are initially located at $x = 2$ and $x = 3$, respectively. Two expansion discontinuities are located at $x = 0.2$ and $x = 4.8$. The exact piecewise solution is

$$u(x,t) = \begin{cases} 0.0, & -\infty < x < 0.2, \\ (x-0.2)/t, & 0.2 < x < t + 0.2, \\ 1.0, & t + 0.2 < x < 2 + 0.25t, \\ -0.5, & 2 + 0.25t < x < 3 - 0.75t, \\ -1.0, & <3 - 0.75t < x < 4.8 - t, \\ (x-4.8)/t, & 4.8 - t < x < 4.8, \\ 0.0, & 4.8 < x < +\infty \end{cases} \tag{50}$$

for $t < 1.0$ and

$$u(x,t) = \begin{cases} 0.0, & -\infty < x < 0.2, \\ (x-0.2)/t, & 0.2 < x < t + 0.2, \\ 1.0, & t + 0.2 < x < 2 + 0.25t, \\ -1.0, & <3 - 0.75t < x < 4.8 - t, \\ (x-4.8)/t, & 4.8 - t < x < 4.8, \\ 0.0, & 4.8 < x < +\infty \end{cases} \tag{51}$$

for $t > 1.0$.

The two shocks moving in opposite directions collide at $t = 1.0$ and a stagnant shock forms. The two expansion fans expand at faster speeds after the respective shocks.

Figure 7 shows the computed results of the three CSL3-type schemes before the collision ($t = 0.75$). The correct positions of the two shocks are obtained. The expansion waves are also accurately computed. The CIP–CSL3_HYMAN produces significant overshoots and undershoots near the shocks as can be expected. CIP–CSL3_UNO and CIP–CSL3_CW give little to be distinguished from each other and produce exceptionally good results. More detailed observations can be obtained from Table VI. All schemes again demonstrate the exact conservation of the first moment. A small amount of overshoot (less than 0.6%) is observed just behind the right-moving shock wave for CIP–CSL3_UNO and CIP–CSL3_CW and is less than that of CIP–CSL3_HYMAN by at least one order. No undershoot is found for CIP–CSL3_UNO and CIP–CSL3_CW. The CIP–CSL3_HYMAN appears more oscillatory but has less l_2 error.

Calculations were continued until $t = 2.0$. The two moving shocks had collided and a single stagnant shock established. Again all the schemes compute correctly the shock and the expansion fans as displayed in Fig. 8.

TABLE VI
Numerical Properties of Different Schemes Applied to the Burgers Equation (Test 7 at t = 0.75)

Scheme	RFM	RSM	MAX	min	E_{l_2}
CSL3_HYMAN	1.0	0.895	1.083	−1.053	1.207×10^{-3}
CSL3_UNO	1.0	0.895	1.006	−1.0	1.765×10^{-3}
CSL3_CW	1.0	0.895	1.005	−1.0	1.759×10^{-3}

Note. The displayed quantities are the same as those in Table I.

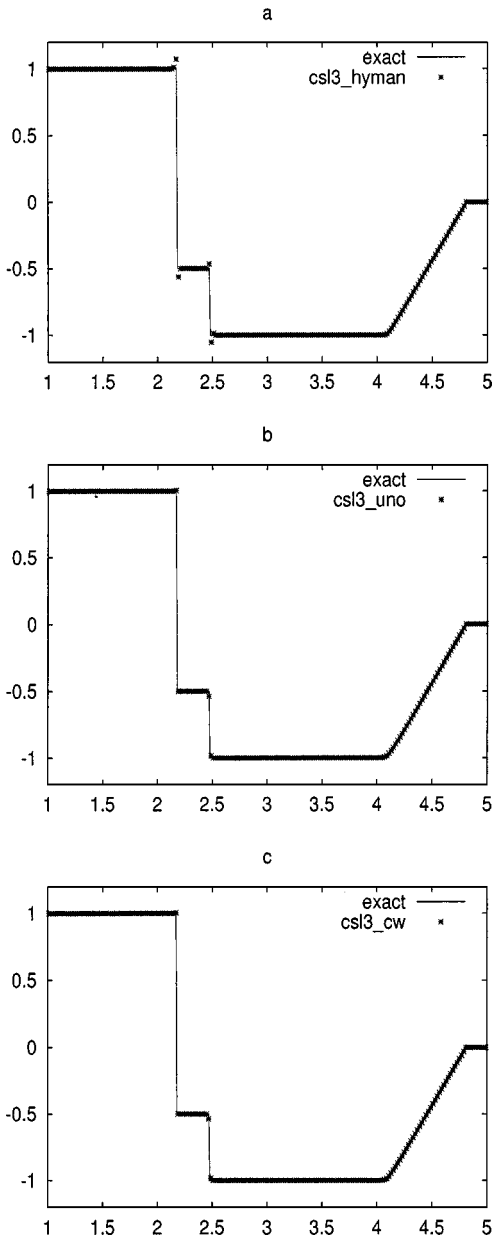

FIG. 7. Solution of the Burgers equation at $t = 0.75$ with an initial condition defined by (49). Displayed are the results computed by the CIP–CSL3_HYMAN scheme (a), the CIP–CSL3_UNO scheme (b), and the CIP–CSL3_CW scheme (c).

4. IMPLEMENTATION WITH LARGE CFL NUMBER

Since the presented schemes are substantially of semi-Lagrangian type, extending the schemes to the large CFL number case is straightforward. As with any other semi-Lagrangian method, the departure points need to be determined as the first step. Accurately estimating the departure point proves important especially when a large time increment is used for

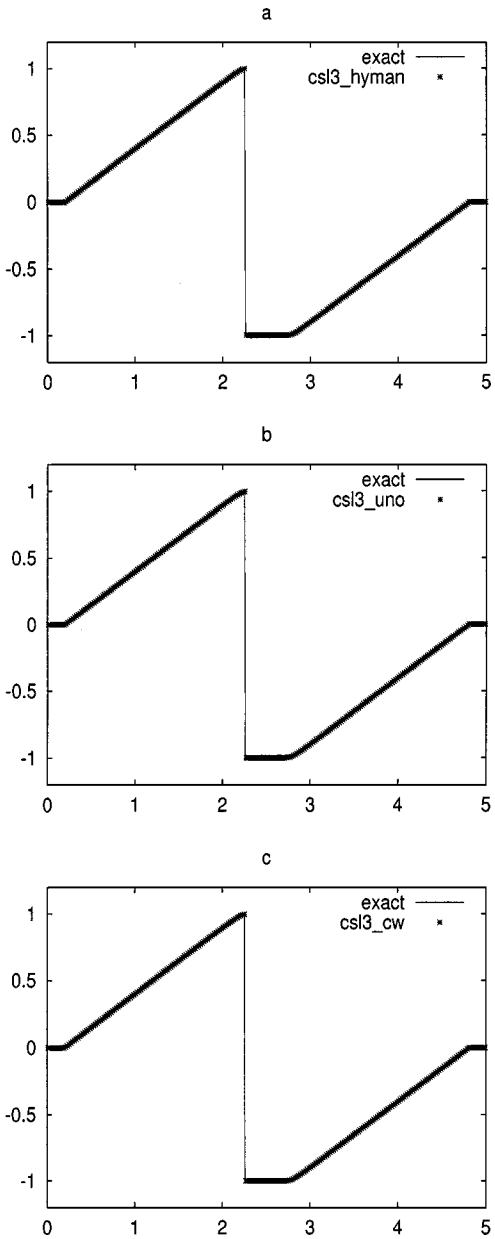

FIG. 8. Same as Fig. 7, but at $t = 2.0$.

integration. For a problem where velocities change with time, an iteration procedure is usually involved to determine the departure position [16, 17], and this leads to high computational overhead. In the following calculations, using a velocity that remains constant, we evaluate the departure point by a Taylor expansion up to fourth order in the space [18],

$$xp(i) = x_i - u\Delta t + \frac{1}{2}\Delta t^2 u\frac{\partial u}{\partial x} - \frac{1}{6}\Delta t^3 u\frac{\partial}{\partial x}\left(u\frac{\partial u}{\partial x}\right) + O(\Delta t^4). \tag{52}$$

The departure point $xp(i)$ may be located at a distance of more than one grid spacing away from the arrival point x_i in case of large CFL number. Suppose $xp(i)$ falls in between grid points $ip(i)$ and $ip(i)-1$ for $xp(i) \le x_i$, or between $ip(i)$ and $ip(i)+1$ for $xp(i) > x_i$. Then the interpolation construction presented in Section 2 can be used by replacing i with $ip(i)$. The advected quantity f is then advanced by

$$\tilde{f}_i = \begin{cases} F^L_{ip(i)}(xp(i) - x_{ip(i)}), & \text{if } xp(i) < x_i, \\ F^R_{ip(i)}(xp(i) - x_{ip(i)}), & \text{if } xp(i) > x_i, \end{cases} \tag{53}$$

and

$$f_i^{n+1} = \tilde{f}_i - \tilde{f}_i \Delta t \left(\overline{\frac{\partial u}{\partial x}} \right)^{\overline{xp(i), x_i}}, \tag{54}$$

where $F^L_{ip(i)}$ and $F^R_{ip(i)}$ represent the interpolation functions over cells $[ip(i)-1, ip(i)]$ and $[ip(i), ip(i)+1]$, respectively. The notation $\overline{(\ )}^{\overline{xp(i), x_i}}$ stands for the averaging along the trajectory $\overline{xp(i), x_i}$. A simple formulation can be written as

$$\left(\overline{\frac{\partial u}{\partial x}} \right)^{\overline{xp(i), x_i}} = \frac{1}{2} \frac{u_{i+1} - u_{i-1}}{\Delta x_{i-1/2} + \Delta x_{i+1/2}} + \frac{1}{2} \frac{u_{ip(i)+1} - u_{ip(i)-1}}{\Delta x_{ip(i)-1/2} + \Delta x_{ip(i)+1/2}}. \tag{55}$$

As discussed in a previous paper [35], the cell-integrated average $\rho_{i-1/2}$ can be advanced by mapping the corresponding quantity in the region between $xp(i)$ and $xp(i-1)$ as

$$\rho^{n+1}_{i-1/2} = g_{ip(i-1)} + \sum_{j=ip(i-1)+1}^{ip(i)} \rho^n_{j-1/2} - g_{ip(i)}. \tag{56}$$

We should note that the semi-Lagrangian feature of our schemes removes the restriction on the time step resulting from the computational stability; however, a large CFL number tends to cause significant numerical errors when velocity violently changes. Furthermore, a criteria for stability in terms of Lipschitz number as discussed in [13, 24] applies to the schemes presented.

The schemes were tested with the following linear transportation problem with a strongly divergent wind defined by

$$u(x) = -1.0 \operatorname{sign}[\sin(2\pi x)](|\sin(2\pi x)|)^{1/8}. \tag{57}$$

The velocity, as shown in Fig. 9, has the largest divergence associated with a steep gradient around the domain center ($x = 1$). The transported quantity will thus spread out from the central area and concentrate at the two ends.

The schemes were used with different CFL numbers. The oscillation-suppressing schemes, CIP–CSL3_UNO and CIP–CSL3_CW, give quite similar solutions without any undershoot. The solutions computed by the CIP–CSL3_UNO with the CFL numbers 0.2, 1.1, and 2.2, respectively, are displayed in Fig. 10. Again the conservation of the total integrated cell average is retained in all the cases. The scheme is stable even with a CFL number up to 2.2 for this sample problem. The numerical results of large CFL computations appear not much different from those of small time step.

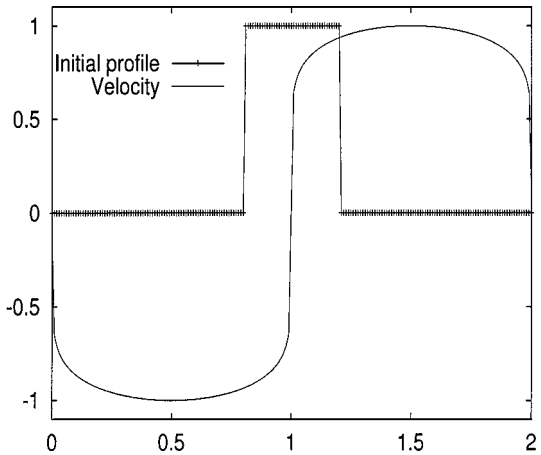

FIG. 9. A test problem with strongly divergent velocity field. Displayed are the velocity defined by Eq. (57) and the initial distribution of the advected quantity.

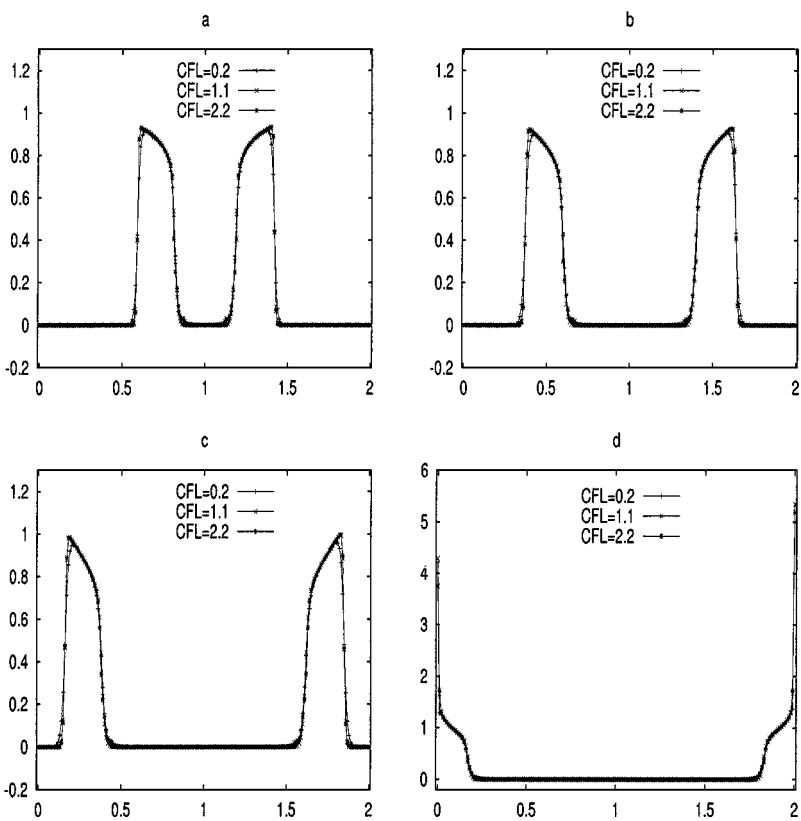

FIG. 10. Advection on a divergent velocity field. Displayed are the results computed by the CIP–CSL3_UNO scheme with different CFL numbers (0.2, 1.1, and 2.2) at $t = 0.22$ (a), $t = 0.44$ (b), $t = 0.66$ (c), and $t = 0.88$ (d).

5. SUMMARY

A class of semi-Lagrangian schemes based on constrained cubic polynomial has been presented. Two constraints were imposed during the construction of the interpolation function. The conservation of the cell-integrated average of the interpolation function was included as a constrained condition to enforce the conservation of the semi-Lagrangian solution. As another constraint, the first-order derivative of the interpolation function at each cell center was introduced to allow the use of manipulations, such as slope limiters, to get oscillationless solutions.

This formulation provides many choices for determining the cell-center slope $d_{i-1/2}$, and allows further investigations. Using the UNO and Collela and Woodward's reconstructions, we obtained completely conservative and oscillationless solutions to linear transportation problems. The conservative constraint guarantees the correct shock positions when applied to nonlinear applications, while the monotonicity of a nonlinear solution requires some extra modifications on the numerical flux involved in the cell-integrated average calculation.

The CIP (*constrained interpolation profile*) concept provides a general methodology for constructing interpolation function. Although this work focuses on the transportation equation, formulations that involve other physical processes should be worthy of investigatation as well.

ACKNOWLEDGMENTS

The authors acknowledge the helpful discussions with Dr. T. Nakamura and Mr. R. Tanaka.

REFERENCES

1. H. Akima, A new method of interpolation and smooth curve fitting based on local procedures, *J. Assoc. Comput. Mach.* **17**, 589 (1970).
2. R. Bermejo and A. Staniforth, The conversion of semi-Lagrangian advection schemes to quasi-monotone schemes, *Mon. Weather Rev.* **120**, 2622 (1992).
3. J. P. Boris and D. L. Book, Flux corrected transport. I. SHASTA: A fluid transport algorithm that works, *J. Comput. Phys.* **11**, 38 (1973).
4. P. Collela and P. R. Woodward, The piecewise parabolic method (PPM) for gas-dynamical simulations, *J. Comput. Phys.* **54**, 174 (1984).
5. D. R. Durran, *Numerical Methods for Wave Equations in Geophysical Fluid Dynamics* (Springer-Verlag, New York, 1999).
6. F. N. Fritsch and J. Butland, *An Improved Monote Piecewise Cubic Interpolation Algorithm*, Lawrence Livermore National Laboratory preprint UCRL-85104, 1980.
7. A. Harten, B. Engquist, S. Osher, and S. R. Chakravarthy, Uniformly highorder accuracy essentially nonoscillatory schemes, III, *J. Comput. Phys.* **71**, 231 (1987).
8. A. Harten and S. Osher, Uniformly high order accurate non-oscillatory schemes, I, *SIAM J. Numer. Anal.* **24**, 279 (1987).
9. P. Holnicki, A piecewise-quintic interpolation scheme, *J. Comput. Phys.* **127**, 316 (1996).
10. J. H. Hyman, Accurate monotonicity preserving cubic interpolations, *SIAM J. Sci. Stat. Comput.* **4**, 645 (1983).
11. G. S. Jiang and C. W. Shu, Efficient implementation of ENO schemes, *J. Comput. Phys.* **126**, 202 (1996).
12. P. D. Lax and B. Wendroff, Systems of conservation laws, *Commun. Pure Appl. Math.* **13**, 217 (1960).
13. S. J. Lin and R. B. Rood, Multidimensional flux-form semi-Lagrangian transportation schemes, *Mon. Weather Rev.* **124**, 2046 (1996).

14. X. D. Liu, S. Osher, and T. Chan, Weighted essentially non-oscillatory schemes, *J. Comput. Phys.* **115**, 200 (1994).
15. A. McDonald, Accuracy of multiply-upstream, semi-Lagrangian advection schemes, *Mon. Weather Rev.* **112**, 1267 (1984).
16. A. McDonald, Accuracy of multiply-upstream, semi-Lagrangian advection schemes, II, *Mon. Weather Rev.* **115**, 1446 (1987).
17. A. McDonald and J. R. Bates, Improving the estimate of the departure point position in a two-time-level semi-Lagrangian and semi-implicit model, *Mon. Weather Rev.* **115**, 737 (1987).
18. J. L. McGregor, Economical determination of departure points for semi-Lagrangian models, *Mon. Weather Rev.* **121**, 221 (1992).
19. G. Moretti, A technique for integrating two-dimensional Euler equations, *Comput. Fluids* **15**, 59 (1987).
20. S. Osher, Riemann solvers, the entropy condition, and difference approximations. *SIAM J. Numer. Anal.* **31**, 217 (1984).
21. A. Priestley, A quasi-conservation version of the semi-Lagrangian advection scheme, *Mon. Weather Rev.* **121**, 621 (1993).
22. D. K. Purnell, Solution of the advective equation by upstream interpolation with a cubic spline, *Mon. Weather Rev.* **104**, 42 (1975).
23. K. Sakurai, T. Aoki, and T. Yabe, A semi-Lagrangian cubic interpolated propagation scheme for long parcel trajectories, *CFD J.* in press.
24. P. K. Smolarkiewicz and J. A. Pudykiewicz, A class of semi-Lagrangian approximations for fluids, *J. Atmos. Sci.* **49**, 2082 (1992).
25. A. Staniforth and J. Côté, Semi-Lagrangian integration scheme for atmospheric model—A review, *Mon. Weather Rev.* **119**, 2206 (1991).
26. L. L. Takacs, A two-step scheme for advection equation with minimized dissipation and dispersion errors, *Mon. Weather Rev.* **113**, 1050 (1985).
27. R. Tanaka, T. Nakamura, and T. Yabe, Constructing exactly conservative scheme in a non-conservative form. *Comput. Phys. Commun.* **126**, 232 (2000).
28. B. van Leer, Toward the ultimate conservative difference scheme. Part IV. A new approach to numerical convection, *J. Comput. Phys.* **23**, 276 (1977).
29. B. van Leer, Toward the ultimate conservative difference scheme. Part V. A second order sequel to Godunov's method, *J. Comput. Phys.* **32**, 101 (1979).
30. D. L. Williamson and P. J. Rasch, Two-dimensional semi-Lagrangian transport with shape-preserving interpolation, *Mon. Weather Rev.* **117**, 102 (1989).
31. F. Xiao, A class of single-cell high order semi-Lagrangian advection schemes, *Mon. Weather Rev.* **128**, 1165 (2000).
32. F. Xiao, T. Yabe, and T. Ito, Constructing oscillation preventing scheme for advection equation by rational function, *Comput. Phys. Commun.* **93**, 1 (1996).
33. T. Yabe and T. Aoki, A universal solver for hyperbolic-equations by cubic-polynomial interpolation. 1. One-dimensional solver, *Comput. Phys. Commun.* **66**, 219 (1991).
34. T. Yabe, T. Ishikawa, P. Y. Wang, T. Aoki, Y. Kadota, and F. Ikeda, A universal solver for hyperbolic-equations by cubic-polynomial interpolation. 2. 2-dimensional and 3-dimensional solvers, *Comput. Phys. Commun.* **66**, 233 (1991).
35. T. Yabe, R. Tanaka, T. Nakamura, and F. Xiao, Exactly conservative semi-Lagrangian scheme (CIP-CSL) in one dimension, *Mon. Wea. Rev.* **129**, 332 (2001).
36. H. Q. Yang and A. J. Przekwas, A comparative study of advanced shock-capturing schemes applied to Burger's equation, *J. Comput. Phys.* **102**, 139 (1992).
37. S. T. Zalesak, Fully multidimensional flux corrected transport algorithm for fluids, *J. Comput. Phys.* **31**, 335 (1979).